Kashani, M. M., Crewe, A. J., & Alexander, N. A. (2017). Structural capacity assessment of corroded RC bridge piers. *Proceedings of the ICE - Bridge Engineering*, *170*(1), 28-41. https://doi.org/10.1680/jbren.15.00023

Structural capacity assessment of corroded RC bridge piers

Mohammad M. Kashani[1] BSc(Hons) MSc PhD

Adam J. Crewe[2] BEng PhD CEng MICE MIStructE

Nicholas A. Alexander[3] BSc(Eng) CMath MIMA, CSci

Abstract

A new numerical model is developed that enables simulation of the nonlinear flexural response of reinforced concrete (RC) components and sections with corroded reinforcement. The numerical model employs a displacement based beam-column element using the classical Hermitian shape function. The material nonlinearity is accounted for by updating element stiffness matrices using the moment-curvature response of the element section considering uniform stiffness over the element. The cover concrete strength is adjusted to account for corrosion induced cover cracking and the core confined concrete strength and ductility are adjusted to account for corrosion induced damage to the transverse reinforcement. The numerical model is validated against a bench mark experiment on a corroded RC column subject to lateral cyclic loading. The verified model is then used to explore the impact of corrosion on the inelastic response and the residual capacity of corroded RC sections. The results show that considering the effect of corrosion damage on RC sections changes the failure mode of RC columns.

Keywords: Corrosion, RC bridge pier, Nonlinear behaviour, Residual capacity

1. Introduction

Among the different deterioration mechanisms, corrosion of reinforcing steel is the most common reason for the premature deterioration of RC structures in a chloride laden environment. This is an important but untimely threat to the safety of historic engineering structures. This premature loss of structural capacity has serious economic cost implications in developed countries. In the UK, the Department of Transport (DoT) estimated that salt-induced corrosion damage on motorway and trunk road bridges totalled £616.5 million in

[1]Lecturer, University of Bristol, Dept. of Civil Engineering University of Bristol, Bristol, BS8 1TR, United Kingdom (corresponding author), E-mail: mehdi.kashani@bristol.ac.uk

[2]Reader, University of Bristol, Dept. of Civil Engineering University of Bristol, Bristol, BS8 1TR, United Kingdom

[3]Senior Lecturer, University of Bristol, Dept. of Civil Engineering University of Bristol, Bristol, BS8 1TR, United Kingdom

England and Wales alone (Wallbank, 1989) and these bridges represent only about 10% of the total bridge inventory in the country. The American Transportation Research Board also reported that there is $150 billion worth of corrosion damage on their interstate highway bridges caused by de-icing and sea salt-induced corrosion (Hida et al., 2010). In 2013, ASCE reported that about 11% of the US bridges were classified as structurally deficient and 24.4% defined as functionally obsolete (ASCE, 2013). Their estimate indicates that the current cost to repair or replace of deficient bridges only is about $76 billion. This total is up from 2009 when the total cost was $71 billion (ASCE, 2013).

Corrosion leads to loss of the steel within the cross section, and a weakening of the bond and anchorage between concrete and reinforcement. This directly affects structural serviceability and strength. Many corroded bridges are also located in regions with high seismic activities. These structures experience dynamic/cyclic loading due to earthquake over their service life. Therefore, corrosion can significantly increase the seismic risk of deteriorating structures. Additionally, this increased vulnerability may be seen at all performance levels; and so it can increase the Whole Life Cycle Cost (WLCC) of the structure. Moreover, the current design approach allows reinforced concrete (RC) structures to dissipate energy during large earthquake events by utilising plastic hinges. Among RC components, bridge piers are the most vulnerable components in earthquakes due to the simple structural form of bridges.

Several researchers investigated the effect of corrosion on the stress-strain behaviour of reinforcing bars in tension (Apostolopoulos, 2007; Apostolopoulos et al., 2006; Du et al., 2005a,b; Cairns et al., 2005). Kashani et al. (2013a-c), Kashani et al. (2014) and Kashani et al. (2015a-c) conducted a comprehensive experimental and computational study on the inelastic behaviour of isolated corroded reinforcing bars. This included the impact of corrosion on inelastic buckling and degradation due to low-cycle fatigue. These results are in good agreement with the results observed of other researchers who studied the cyclic behaviour of RC components.

Moreover, in recent years, several researchers have studied the seismic vulnerability and fragility analysis of corroded RC bridges (Alipour et al., 2011; Choe et al. 2008; Ghosh and Padgett, 2010). They have investigated the effect of reinforcement corrosion on the nonlinear behaviour and response of RC bridges subject to seismic loading. These studies used nonlinear fibre-based finite element analyses (OpenSees, 2014). However, they have used very simple uniaxial material models to model the impact of corrosion on the stress-strain behaviour of reinforcing steel. In most cases the corrosion damage has only been limited to

the reinforcing steel by considering an average reduced area and/or reduced yield strength. Furthermore, the impact of corrosion on ductility loss, the inelastic buckling of vertical reinforcement and corrosion induced damage to cover and core confined concrete are ignored.

In this paper a computational technique is developed that enables simulation of the nonlinear flexural response of RC components with corroded reinforcement. The model employs a new uniaxial material model for corroded reinforcing steel. This model simulates the stress-strain behaviour of corroded reinforcing steel with the effect of inelastic buckling (Kashani et al., 2015a). The computational model is validated against a bench mark test on a representative corroded RC column. The result of the experimental testing of the corroded column and verification of the computational model are reported in this paper. Finally, the verified model is used to investigate the effect of corrosion on the nonlinear response and residual capacity of corrosion damaged RC sections.

2. Experimental Programme

In order to investigate the effect of corrosion on the nonlinear behaviour of RC components a comprehensive set of experimental testing proposed. Firstly, the influence of corrosion on nonlinear stress-strain behaviour of reinforcing bars under monotonic (tension and compression including the effect of inelastic buckling) and cyclic loading was explored. The experimental testing conducted on about 150 test corroded reinforcing bar specimens which followed by numerical modelling of experimental specimens. The outcomes of these studies are reported in separate publications (Kashani et al., 2013a-c; Kashani et al., 2014, Kashani et al. 2015b-c). Using the experimental results, an advanced uniaxial material model for the simulation of the stress-strain behaviour of corroded reinforcing bars is developed (Kashani; 2014; Khashani et al., 2015a). This new material model is used in development of a computational technique to model the nonlinear behaviour of RC sections and components and is reported in section 3 of this paper.

The second part of this research programme is a bench-mark reaction wall test on a prototype corroded RC column. The results of this experiment are used for validation of the computational model. The next section (section 2.1) reports the details and results of this experiment.

2.1 Reinforced concrete column specimen

A RC column 250mm by 250mm in cross section and 2500mm high (height above the foundation) was designed to EC2 criteria. There are 8 12mm diameter vertical bars in the column section with 8mm diameter horizontal tie reinforcement. The tie reinforcement is spaced at 50mm up to the 800mm above the foundation and thereafter 150mm. The column and foundation were cast separately and after completion of the corrosion process the column was cast into the foundation. The cover concrete was 25mm and the maximum aggregate size of concrete was 10mm. Figure 1 shows the details of the column test specimen and Table 1 and Table 2 summarise the mechanical properties of the steel and concrete used in this test specimen

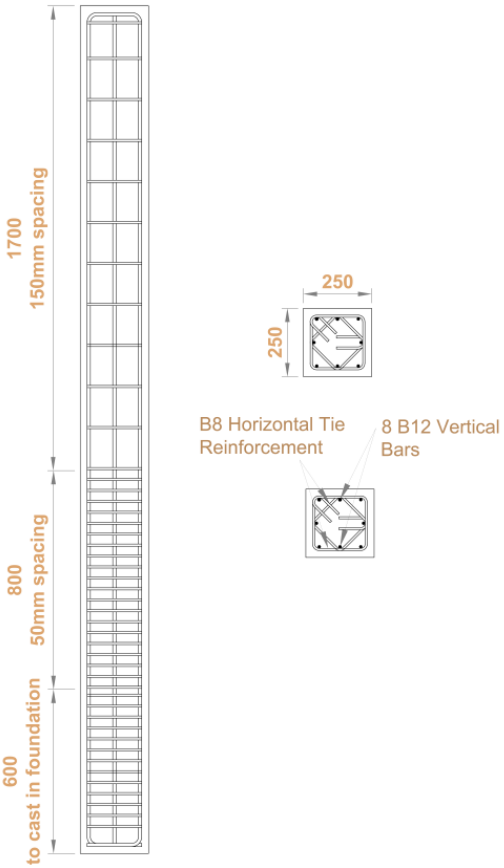

Figure 1 Reinforcement details of RC column test specimen

It should be noted that this column is not intended to represent the full scale bridge pier. This column is representative of typical RC columns designed to EC2 to investigate the impact of corrosion. The dimension of the column is chosen in a way that is reasonably large and also reasonably easy to break using our high-performance actuators. Larger size column could be chosen but it required large actuator for the structural testing. In terms of slenderness, we tried to make the column to be flexural governed to avoid any significant nonlinear shear

deformation. The material testing showed that the scale doesn't affect the stress-strain behaviour of materials used in this experiment. This is because they are still within the normal range of materials in typical RC construction. It should be noted that the stress-strain behaviour of reinforcement is not affected by the bar diameter and cube tests showed that stress-strain behaviour of concrete didn't affected by reduced aggregate size (see Table 2). Therefore, the scaling will not affect the results.

Table 1 Mechanical properties of uncorroded reinforcement

Reinforcement type		**8 mm (B8)**	**12mm (B12)**
Yield Strength	f_y (MPa)	510	540
Modulus of Elasticity	E_s (Mpa)	194881	212099
Yield Strain	$\varepsilon_y = f_y/E_s$	0.00261	0.00254
Ultimate Strength	f_u (MPa)	645	616
Ultimate Strain at Maximum Stress	ε_u	0.04660	0.06033
Strain Ratio	$\varepsilon_u/\varepsilon_y$	17.85	24.42
Strength Ratio	f_u/f_y	1.27	1.18
Total Elongation at Maximum Force	λ (%)	4.66%	6.03%
Total Elongation at Failure	λ_f (%)	7.01%	16.1%
Unit Mass	m (kg/m)	0.396	0.874

Table 2 Properties of concrete

	W/C	**Max Aggregate Size**	**Maximum Strength**
Concrete	0.45	10 (mm)	30 (MPa)

2.2 Accelerated corrosion procedure and cyclic reaction wall test

The RC column was first subjected to an accelerated corrosion process by applying an anodic current of specified intensity and time. This comprised an electrochemical circuit using an external power supply. The reinforcing bars act as an anode in the cell and an external material acts as the cathode. In this experiment stainless steel is used as the external material. Only the part of column which would be immediately above the foundation (800mm above base level) was immersed in 5% NaCl solution in a tank. A data acquisition system was set up to monitor the current and voltage applied to the column during the test. After completion of the accelerated corrosion the column was cast into the foundation block.

The predicted percentage mass loss using Faraday's law of electrolysis (Kashani et al. 2013a) was 15% mass loss after applying an average of 3A current for 4 months. The power supply was set to 3A current; however, the monitoring data showed that an average of 2.15A current

was applied over the 4 months. The actual mass loss of corroded reinforcement inside the concrete was calculated by measuring the actual mass of corroded reinforcement after the reaction wall test. This procedure required the demolition of the RC column after the cyclic testing. Figure 2 (a) shows the accelerated corrosion procedure in the laboratory and Figure 2 (b) shows the corroded column after completion of the accelerated corrosion process. The mass loss measurement of corroded reinforcement after the reaction wall test showed an average of 6.1% mass loss. This is because the Faraday's law is based on bare steel not steel inside concrete. Therefore there will be some differences between the theoretical faraday's law and the experimental results. If the corrosion rate is low there will be better agreement between the corrosion of bars inside concrete and Faraday's law. Moreover, the applied current is distributed between the longitudinal and transverse bars. Therefore, The Faraday's law predicts the total mass loss of the steel in the electrical circuit and it will be different from the mass loss of individual bars. The detailed discussion is available in Kashani et al. (2013a)

The lateral cyclic load was applied by a 50kN actuator. Lateral deflection over the height of the column, rotation at the base and strains were measured using external displacement transducers. The reaction wall test set up is shown in Figure 2 (c). No axial force was applied in this experiment. The experiment was conducted under displacement control system. A two cycle reversed symmetrical displacement history was used in these experiments. The actuator was set to displacement control with a constant displacement rate of 2 mm/s.

(a)

(b)

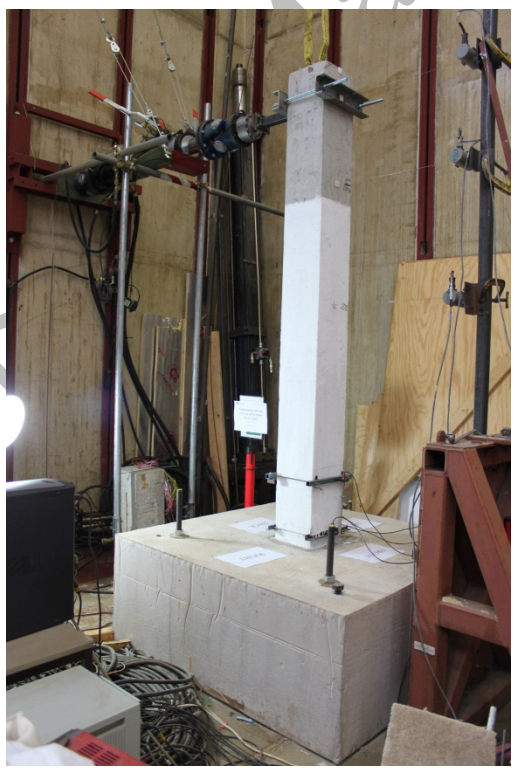

(c)

Figure 2 Corroded column specimens: (a) accelerated corrosion process, (b) corroded column after accelerated corrosion procedure and (c) reaction wall test setup in the laboratory

2.3 Experimental results and discussion

The force-lateral displacement response of the corroded column specimen is shown in Figure 3. Figure 4 shows the development of flexural damage as the drift level is increased during the test. The first flexural cracks appeared at a displacement of 15 mm corresponding to 0.6% drift. The maximum measured positive load was 20.3kN at 3% drift (75mm), the maximum measured negative load was 20kN at 3% drift (75mm).

Horizontal cracks appeared during cycles between 0.6% and 5.0% drift, growing in number and extension, and were located at the column base, and up to the height about 700mm from the top of the foundation (Figure 4(a)). The crack density and widths were concentrated in the lower 250mm of the column which corresponds to the plastic hinge length. Some minor vertical cracks along the vertical bars were observed. These cracks were initially caused by the corrosion and opened up during the cyclic test. The corrosion level in this experiment was only moderate otherwise these cracks could be opened up more significantly as observed by other researchers (Meda et al. 2014; Ma et al. 2012).

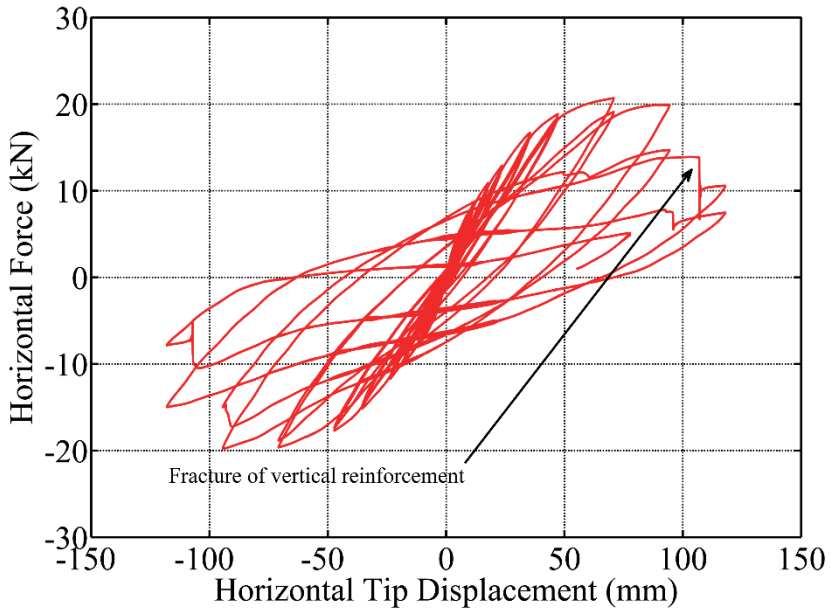

Figure 3 Result of the reaction wall test: (a) loading protocol and (b) cyclic force-displacement response

(a)

(b)

(c)

(d)

(e)

Figure 4 Development of flexural damage in the corroded column: (a) 0.6% drift (b) 1.0% drift (c) 3.0% drift (d) 4.5% drift and (e) close view of corroded bar fracture in tension

After the peak horizontal force a significant strength reduction and degradation was seen in the force-displacement response. The first significant strength loss was seen at 4.5% drift (112.5mm). The measured horizontal force at this cycle was 13kN, which was 65% of the maximum measured load. At this point the first vertical bar fractured in tension. Figure 4(d)

shows the severe crack opening at 4.5% drift which is due to the fracturing of a corner bar. Figure 4(e) shows the fracture of vertical bar in tension. This type of failure in RC components under cyclic loading is due to the low-cycle high amplitude fatigue degradation (Kashani et al., 2015b).

Following the fracturing of the first vertical bar a significant reduction was seen in the force-displacement response of the column. This was then followed by a sharp degradation in force-displacement response. As the first bar fracture was located in the corner of the column this resulted in a significant loss of strength and permanent damage that caused the column to tilt sideway. As a result the column only sustained two cycles after fracture of first vertical bar and therefore the test was stopped at this point. It should be noted that the column was well confined and therefore the buckling of vertical bars was not seen and the failure was governed by fracture of bars in tension.

3. Computational modelling for nonlinear response prediction of corroded RC columns

In recent years, for nonlinear analysis of RC structures subject to seismic loading, a lot of attention has been given to the development of the fibre element technique (Spacone et al., 1996a,b). In this method the member cross section is discretised into a number of steel and concrete fibres at section level. The material nonlinearity is then considered through the uniaxial constitutive material models of steel (tension and compression) and concrete (confined core concrete and unconfined cover concrete). Given that the stiffness of reinforced concrete beam-column elements (frame elements) varies with the loading, element response is greatly influenced by the moment-curvature (M - κ) response of the cross section. Therefore, the element stiffness matrix in the fibre element technique is estimated based on the $M - \kappa$ response of element cross sections.

3.1 Computation of moment-curvature for a beam-column section

The theoretical force-moment-curvature (F - M - κ) relationship is obtained as follows. The main assumptions here are that plane sections remain plane and the interaction effects of shear stress and direct stress are assumed to be negligible (Euler-Bernoulli beam theory). Here a compression-positive sign convention is used. Figure 5 shows a schematic overview of the F - $M - \kappa$ relationship.

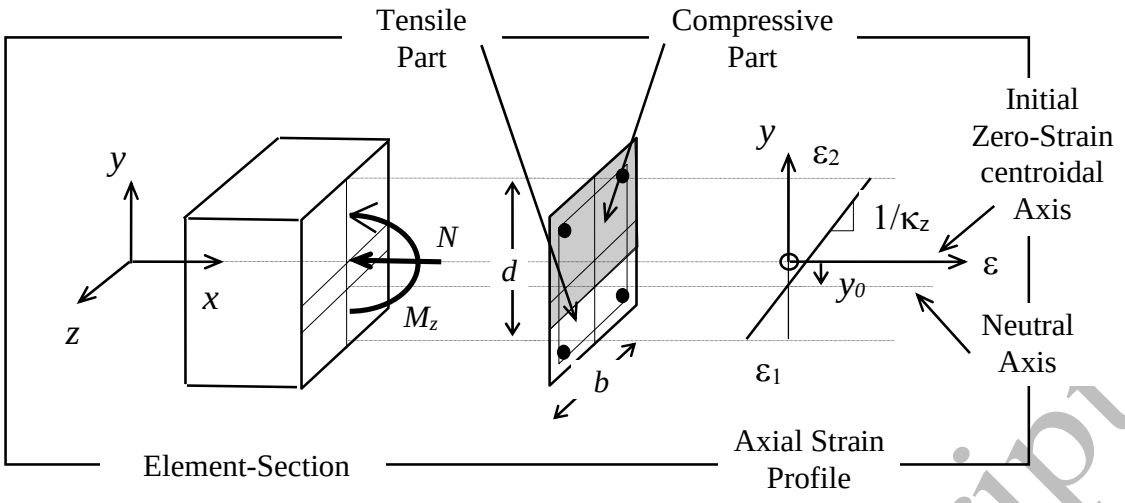

Figure 5 (M - κ) relationship of RC sections

The linear strain distribution is given by the following

$$\varepsilon(y) = y\kappa_z + \varepsilon_0 \qquad \text{and} \qquad \varepsilon_0 = \left(\frac{\varepsilon_2 + \varepsilon_1}{2}\right) \qquad \kappa_z = \frac{\varepsilon_2 - \varepsilon_1}{d} \tag{1}$$

The direct stress for steel is $\sigma_s = f_s(\varepsilon)$ where the function f_s is defined by the new uniaxial material model developed by Kashani et al. (2015a). The direct stress for concrete (confined core concrete and unconfined cover concrete) is $\sigma_c = f_c(\varepsilon)$ where the function f_c is defined by Park et al. (1982) equations for confined and unconfined concrete.

By considering equilibrium between internal and external actions

$$N = \int \sigma dA \quad \text{hence} \quad N = \underbrace{\int \sigma_c b dy}_{Concrete} + \underbrace{\sum \sigma_s \Delta A_s}_{Steel\ bars} - \underbrace{\sum \sigma_c \Delta A_s}_{voids},$$

$$S_N \equiv \left\{\int \sigma_c b dy + \sum (\sigma_s - \sigma_c)\Delta A_s - N\right\} = 0 \tag{2}$$

$$M_z = \int y\sigma dA \quad \text{hence} \quad M_z = \underbrace{\int y\sigma_c b dy}_{Concrete} + \underbrace{\sum y\sigma_s \Delta A_s}_{Steel\ bars} - \underbrace{\sum y\sigma_c \Delta A_s}_{Voids}$$

$$S_{M_z} \equiv \left\{\int y\sigma_c b dy + \sum y(\sigma_s - \sigma_c)\Delta A_s - M_z\right\} = 0 \tag{3}$$

The concrete stress integrals $\int \sigma_c b dy$ & $\int y\sigma_c b dy$ can be evaluated numerically using the trapezium rule given a specific strain profile. Equations (2) and (3) represent two simultaneous non-linear equations in terms of *parameters* (a) strain ε_0 (b) curvature κ_z (c) applied axial force N (d) applied moment M_z (e) location and size of steel bars (f) stress-strain table for steel (g) size and geometry of concrete section, including possible variation in width b (h) stress-strain table for concrete (including tensile strains). Given sectional and

reinforcement details including material stress-strain tables, the action N and the curvature κ_z: equations (2) and (3) can be solved for parameters strain ε_0 and M_z. A 1D iterative scheme using *Newton-Raphson* algorithm is used to solve this system of equations. Once the solution strain profile is determined the flexural-rigidity and axial rigidity can be calculated.

$$EI_z = \frac{M_z}{\kappa_z}, \quad EA = \int EdA \quad \text{hence} \quad EA = \underbrace{\int E_c b dy}_{Concrete} + \underbrace{\sum E_s \Delta A_s}_{Steel\ bars} - \underbrace{\sum E_c \Delta A_s}_{Voids} \tag{4}$$

By executing the above algorithm for a range of curvature values the moment-curvature relationship can be derived. Allowance can also be made for buckling of the compression bars (Kashani et al. 2014). The effective length, L/D, used in the buckling model was taken as the ratio of tie spacing (L) to vertical bar diameter (D). Thus the reinforcing bars are allowed to buckle when the strain in the concrete is great enough to cause spalling and when the force levels in the bar exceed the critical buckling load. If no allowance is made for this effect then the theoretical moment curvature relationship shows strain hardening.

3.2 Nonlinear finite element model using beam-column element

For the column model the typical displacement-based beam-column element using Hermitian shape functions is used (Bathe, 1996). To account for the second order effect due geometrical nonlinearity the geometric stiffness matrix is added to the material stiffness matrix (McGuire, 2000). To model the slippage of the reinforcement at the interface of the column and foundation a rotational spring model is used. Figure 6 shows a schematic overview of the proposed finite element model. The w in Figure 6 is the column width.

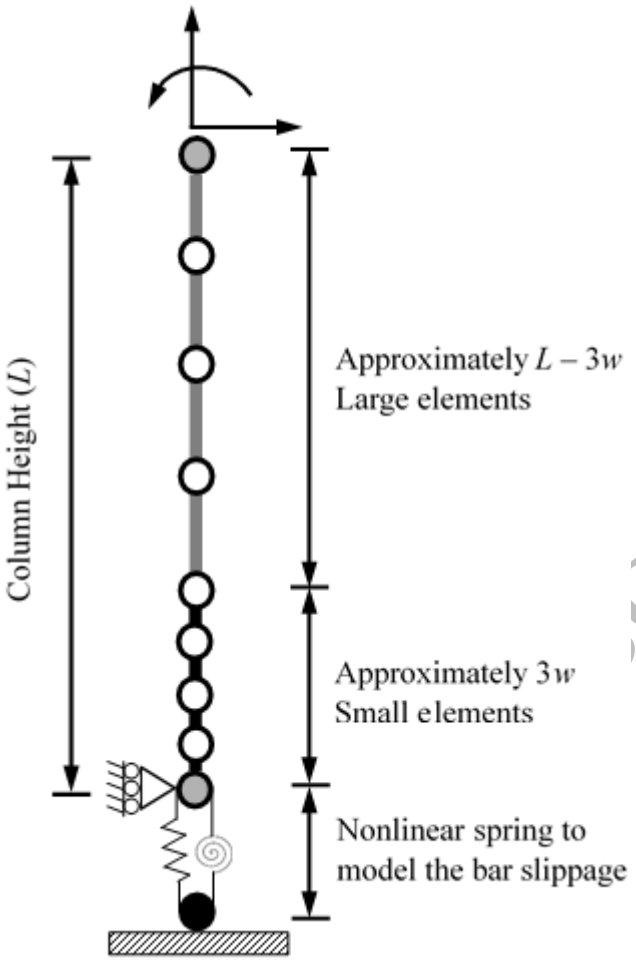

Figure 6 Schematic illustration of the proposed finite element model of RC column

3.3 General solution procedure to account for material nonlinearity

The element stiffness matrices are assembled in the standard way, i.e. local to global transformation, assemblage of global stiffness matrix, introduction of support restraints, production of action vector due to the applied actions and deformations. An incremental loading scheme is used where the applied actions and deformations are increased, incrementally, up to failure of the structure. At each increment the global system of linear equations is solved resulting in nodal displacements (in global coordinates). Element nodal actions can be calculated in the standard way from the element nodal displacements in local co-ordinates. By using the moment-curvature lookup table for a section the internal node moment and hence flexural rigidity can be calculated. Then the element stiffness matrices are updated for the next increment. A Newton-Raphson convergence procedure was not used in this paper, as the increments in displacement are kept small. The details of incremental size verification and mesh sensitivity are available in (Noor et al., 2000; Cox, 2000). In this study 10 elements are used to model the first 800mm height of the column immediately above the

foundation and 5 elements are used to model the rest of the column to the top. It should be noted that the Figure 6 is only indicative and does not represent the actual number of elements used in the analysis.

4. Modelling the impact of corrosion on reinforcing steel and damaged concrete

4.1 Effect of Corrosion on the nonlinear stress-strain behaviour of reinforcing bars

The results of the tension tests showed that corrosion levels of up to about 15% do not have a significant effect on the stress-strain curves. However, once the corrosion level is greater than 15% a significant drop occurs in plastic deformation capacity and the residual capacity of the corroded bars. This is similar to the results from previous studies which used similar reinforcement. Further details and discussion is available in Kashani et al. (2013a) and Du et al. (2005a,b).

To account for the limited strength and ductility capacity of corroded reinforcing bars the stress-strain curve for the reinforcement is modified by changing the yield stress and fracture strain. This empirical change in yield stress and fracture strain (based on experimental data) is described by Equations (5) and (6) below:

$$\sigma'_y = \sigma_y(1-\beta_s\,\psi) \tag{5}$$

$$\varepsilon'_u = \varepsilon_u(1-\beta_e\,\psi) \tag{6}$$

where, σ'_y is the yield stress of a corroded bar in tension, σ_y is the corresponding yield stress of the uncorroded bar and ψ is the percentage mass loss due to corrosion. The value of β_s is 0.005 and β_e is 0.05 as reported by Du et al. (2005a,b). The β_s and β_e are empirical coefficients known as *pitting coefficients* that account for the influence of pitting on the premature fracture and reduced capacity of corroded reinforcing bars.

4.2 Effect of corrosion on inelastic buckling of corroded bars

The empirical equations developed by Kashani *et al*. (2013a) are used to modify the compression response of corroded reinforcement. The effect of corrosion on compressive yield strength (σ'_{yc}) is defined using the empirical Equation (7), which is calibrated based on the observed experimental results:

$$\sigma'_{yc} = \begin{cases} \sigma_y \left(1 - 0.005\,\psi\right) & \text{for } L/D \le 6 \\ \sigma_y \left(1 - 0.0065\,\psi\right) & \text{for } 6 < L/D < 10 \\ \sigma_y \left(1 - 0.0125\,\psi\right) & \text{for } L/D \ge 10 \end{cases} \tag{7}$$

The details of the experimental results and development of the above empirical equations are available in in Kashani et al. (2013a).

4.3 The new nonlinear uniaxial material model for reinforcing bars

Kashani et al. (2015a) developed a new uniaxial material model for reinforcing bars. The new material model accounts for the influence of corrosion damage, inelastic buckling and low-cycle fatigue degradation. The material parameters are calibrated based on experimental and numerical simulation data of uncorroded and corroded bars.

The basic tension envelope is that proposed by Balan et al. (1998) which employs a continuous function that provides a smooth transition from linear elastic to the strain hardening region. This improves the numerical stability during the computational process. Therefore, this model is use to define the tension envelope (Equation (8)).

$$\sigma = \sigma_y \frac{(1-\mu)}{2}\left[1 + \frac{(1+\mu)}{(1-\mu)}\frac{\varepsilon}{\varepsilon_y} - \sqrt{\left(\frac{\varepsilon}{\varepsilon_y}\right)^2 + \delta}\right] \tag{8}$$

where $\mu = E_h / E_s$ is the hardening ratio with E_s and E_h equal to the elastic modulus and hardening modulus for the steel, σ_y is the yield stress, ε is the current strain, ε_y is the yield strain and δ is a shape parameter. Equation (8) represents a hyperbola with two asymptotes, one with slope E_s and one with slope E_h. The shape parameter, δ, defines the curvature radius of the transition between the linear elastic and hardening regions of the curve. Further details of this model are available in Balan et al. (1998).

The basic compression envelope of the model employs an exponential function to describe the post-yield bucking response of the reinforcing bars. This approach has been used previously by others to model the inelastic buckling behaviour of concentric steel bracing (Hill et al., 1989; Thai and Kim, 2011); here the post-buckling curve is defined in Equation (5):

$$\sigma = \begin{cases} E_s\,\varepsilon & : \varepsilon \le \varepsilon_y \\ \sigma^* + \left(\sigma_y - \sigma^*\right)\exp\left(-\left(\rho_1 + \rho_2\sqrt{\varepsilon_p}\right)\left(\varepsilon_p\right)\right) & : \varepsilon > \varepsilon_y \end{cases} \quad \text{for} \quad 8 \le L/D \le 30 \tag{9}$$

where ρ_1 is the initial tangent of the post-buckling response curve, ρ_2 is the rate of change of the tangent, ε is the current strain, $\varepsilon_p = \varepsilon - \varepsilon_y$ is the plastic strain, σ^* is the asymptotic lower stress limit of the post-buckling curve, and all other variables are as previously defined. The parameters ρ_1, ρ_2 and σ^* are defined by the yield strength and the geometrical slenderness ratio of the reinforcing steel, as defined below:

$$\rho_1(\lambda_p) = 4.572\lambda_p - 74.43 \tag{10}$$

$$\rho_2(\lambda_p) = 318.40 \exp(-0.071\lambda_p) \tag{11}$$

$$\sigma^* = 3.75 \frac{\sigma_y}{\frac{L}{D}} \tag{12}$$

$$\lambda_p = \sqrt{\frac{\sigma_y}{100}} \frac{L}{D} \tag{13}$$

where σ_y has units of MPa.

Further discussion and detailed derivation of the above equations are available in Kashani et al. (2015a). The yield and buckling strength and ultimate strain of corroded reinforcement in Equations 8 to 13 is then modified using the empirical formulas described in sections 4.1 and 4.2.

4.4 Modelling the impact of corrosion on geometrical properties of corroded bars

Kashani et al. (2013c) conducted 3D optical measurement of corroded bars to explore the spatial variability of the corrosion pattern. They found that the geometrical properties of corroded bars can be modelled using a lognormal distribution. In this study, the mean values of the lognormal distribution models are used to account for the effect of pitting corrosion on the geometrical properties of corroded bars.

Equation (14) can be used to calculate the average reduced cross section area of reinforcement considering a linear reduction in area as function of percentage mass loss ψ.

$$A_{ave} = A_0(1 - 0.01\psi) \tag{14}$$

where, A_{ave} is the average reduced cross section area of corroded reinforcement and A_0 is the corresponding original uncorroded cross section area.

Once the average reduced cross section area is calculated, the cross section area considering pitting effect (A') can be calculated using the Equation (15).

$$A' = \gamma A_{ave} \tag{15}$$

where, γ is the mean value of area pitting coefficient that is derived by assuming a lognormal distribution. Further detail is available in Kashani et al. (2013c).

Kashani et al. (2013c) found that the irregular cross section shape of the corroded bars results in rotation of principal axis. Therefore, in probabilistic models they considered the minimum principal second moment of area. The minimum second moment of area of the corroded bars ($I'_{\min}$) can be calculated by introducing a pitting coefficient for second moment of area as defined in Equation (16) below:

$$I'_{\min} = \mathrm{K}\, I_0 \tag{16}$$

where, K is the mean value of the pitting coefficient of minimum second moment of area of corroded bars considering lognormal distribution and I_0 is the second moment of area of the original uncorroded bar.

The mean values of the pitting coefficients (γ and K) can be calculated using Equation (17).

$$M_{(\gamma \text{ or } \mathrm{K})} = \exp\left(\mu + \frac{\sigma^2}{2}\right) \tag{17}$$

where, μ and σ are defined in Equations (18) and (19) below:

$$\mu = a\psi^b \tag{18}$$

$$\sigma = c\psi^d \tag{19}$$

The coefficients a,b,c, and d and further detail is available in Kashani et al. (2013c).

4.5 Modelling corrosion induced cracked cover concrete

The response of cracked concrete in compression is described in detail by Vecchio and Collins (1986) which is known as Compression Field Theory (CFT). Based on CFT the compressive strength of cracked concrete in compression depends on the magnitude of the average tensile strain in the transverse direction, which causes longitudinal microcracks. A similar theory applies for the corrosion induced cracking of cover concrete which is in compression. Coronelli and Gambarova (2004) employed this method in nonlinear finite element analysis of corrosion damaged RC beams. Equation (20) can be used to modify the compressive strength of cover concrete as follows:

$$\sigma_c' = \frac{\sigma_c}{1+\eta\frac{\varepsilon_1}{\varepsilon_{c_0}}} \tag{20}$$

where, η is the coefficient related to bar roughness and diameter (for medium-diameter ribbed bars a value η = 0.1); ε_{co}= strain at the peak compressive stress σ_c ; and ε_1=average (smeared) tensile strain in the cracked concrete at right angles to the direction of the applied compression. Further detail is available in Coronelli and Gambarova (2004).

4.6 Modelling corrosion damaged confined concrete

Reinforced concrete bridge piers exhibit inelastic response when they are subjected to large lateral forces during major earthquakes. It is well known that the confinement associated with hoop reinforcement will increase the ductility and energy absorption capacity of RC bridge piers. However, the corrosion of horizontal tie reinforcement can change the behaviour of confined concrete under high compression loads. Here the effect of corrosion on confined concrete is considered by reducing the volumetric ratio and yield strength of the confinement reinforcement as a function of steel mass loss due to corrosion. The influence of corrosion on reduced ductility is also considered by limiting the maximum crushing strain in the confined concrete as a function of reduced ductility of hoop reinforcement by modifying the empirical equation developed by Scott et al. (1982).

Scott et al. (1982) defined the maximum crushing strain of the confined concrete by the fracture of the first horizontal tie/spiral reinforcement. The model proposed by Scott et al. (1982) is defined in Equation (17).

$$\varepsilon_{cc} = 0.004 + 1.4\left(\frac{\rho_{sc}\sigma_{ytie}\varepsilon_{utie}}{\sigma_c}\right) \tag{21}$$

where, ε_{utie} is the fracture strain of the tie/spiral reinforcement, σ_{ytie} is the yield strength of horizontal tie reinforcement and ρ_{sc} is the volumetric ratio of confinement reinforcement i.e. horizontal tie reinforcement. The yield strength, fracture strain and volumetric ratio of horizontal ties reinforcement can be modified using the empirical models described in sections 4.1, 4.2 and 4.4 of this paper.

4.7 Modelling bond-slip behaviour of column-foundation interface

In the seismic design of RC structures and bridges, plastic hinges are formed at the column/beam ends. This will induce a substantial strain penetration along the longitudinal bars into the joint that eventually results in slippage of the longitudinal bars. This

phenomenon was observed in the column experiment and also by other researchers (Lehman and Moehle, 2000). Lowes and Altoontash (2003) adopted a bar-slip model for the end slip of longitudinal reinforcement in beam-column joints.

Corrosion affects the reinforcing steel near the surface of the concrete due to diffusion of chloride ions from the surface and/or carbonation of the cover concrete. In bridge piers, the vertical reinforcement bars are anchored to the foundation well below the foundation surface. Therefore, the vertical reinforcement does not corrode at this depth and the bar-slip behaviour of the bars at the anchorage zone remains the same as in the uncorroded column. This has been observed by other researchers experimentally.

It should be pointed out that corrosion does affect the bond strength of corroded vertical reinforcement above the foundation level (internal bond-slip within the column itself). However, based on the observed experimental results, the reduced bond-strength does not govern the failure of columns. Meda et al. (2014) and Ma et al. (2012) reported that the failure of corroded columns and beams under cyclic loading is mainly governed by fracture of bars in tension due to low-cycle fatigue and buckling of bars and crushing of confined concrete in compression.

Therefore, the bond-slip of corroded vertical bars within the element is not considered in this research. A further detail of development of the bond-slip model is available in Kashani (2014).

5. Validation and discussion of computational results

5.1 Monotonic pushover analysis result

It is assumed that the reinforcing bars (vertical and tie reinforcement) have the same percentage mass loss as measured. Given the column is very well confined the buckling length of the vertical bars is taken to be the same as the spacing of tie reinforcement (L/D =5). This assumption is proved to be correct by the failure mode observed in the experiment (as it is shown in Figure 4). The procedure explained in section 3 together with uniaxial material models described in section 4 have been used in the nonlinear pushover analysis. Figure 7 shows the results of the monotonic pushover analysis of the proposed column and a comparison with the experimental result. The numerical results show that considering the bond-slip of the base of the column does not have a significant impact on the prediction of the maximum strength of column. However, bond-slip influences the plastic rotation capacity i.e. ductility of the column.

The numerical results show that the failure mode starts with cracking of cover concrete followed by fracture of the vertical reinforcement in tension. This is in good agreement with the observed experimental results. The numerical analysis and the experimental results demonstrate the importance of modelling the influence of corrosion on both steel and damaged concrete (through loss of confining tie reinforcement). The corrosion damage of the confined concrete results in a rapid reduction in strength and ductility of the corroded column under cyclic loading. It should be noted that the computational model that is developed in this paper is valuable for the prediction of the capacity of corroded columns. However, it does not account for cyclic degradation and the low-cycle fatigue failure of vertical reinforcing bars. Further discussion about the cyclic degradation and low-cycle fatigue of corroded columns is available in (Kashani, 2014 and Kashani et al., 2015).

The numerical model showed that, in the absent of axial force and inelastic buckling, the failure mode is governed by fracture of vertical bars in tension. However, this may not be valid for columns with axial for with buckling. Therefore, the validated numerical model is used to explore the effect of axial force, inelastic buckling and corrosion damage on the residual capacity of RC column sections. This is reported in section 5.2 of this paper.

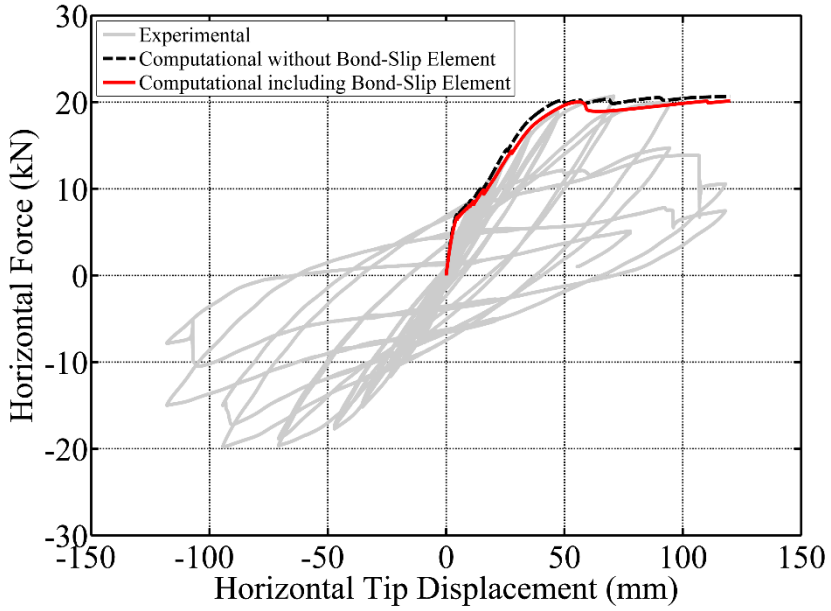

Figure 7 Comparison of the computational response and observed experimental response

5.2 Impact of corrosion on the nonlinear response and capacity of RC sections

The proposed numerical model is validated against a benchmark experimental test. Here, to demonstrate the influence of corrosion on capacity reduction and the inelastic response of RC sections a series of moment-curvature (M-κ) analyses are conducted on the a hypothetical

column with the same cross section properties (dimension, reinforcement etc.) as the tested column. To investigate the combined impact of corrosion and bar buckling on inelastic section response, an L/D = 10 is assumed in the analyses. The results of these analyses are shown in Figure 8. To show the significance of buckling, M-κ analyses are conducted for uncorroded sections with and without the bar buckling effect. The M-κ analyses of corroded sections are only considered with the effect of buckling. Figure 8(a) shows that corrosion has a significant impact on the flexural rigidity and ductility of RC sections. It should be noted that the tested column had no axial force but the axial force-bending moment interaction is included in the numerical model. The impact of axial force on the nonlinear section response is more severe where the inelastic buckling of vertical bars are critical. The high axial force results in spalling of cover concrete at a lower drift ratio and followed by inelastic buckling of vertical bars. Once the vertical bars buckled they loose strength after buckling which subsequently increases the stress in core concrete (concrete confined within hoops). Therefore, the core concrete crushes soon after buckling. This can be seen in Figure 8(a) where it compares the moment curvature response of the hypothetical RC section with and without considering buckling.

In the M-κ analysis if the strain in the extreme fibre is limited to a fixed value i.e. concrete crushing strain in compression, and the M-κ analysis repeated for a range of axial forces, the axial force-bending moment (P-M) interaction diagram can be generated. Figure 8(b) shows the P-M interaction diagram of the same section with a varied corrosion level. It is evident from Figure 8(b) that corrosion has a significant impact on capacity of RC sections.

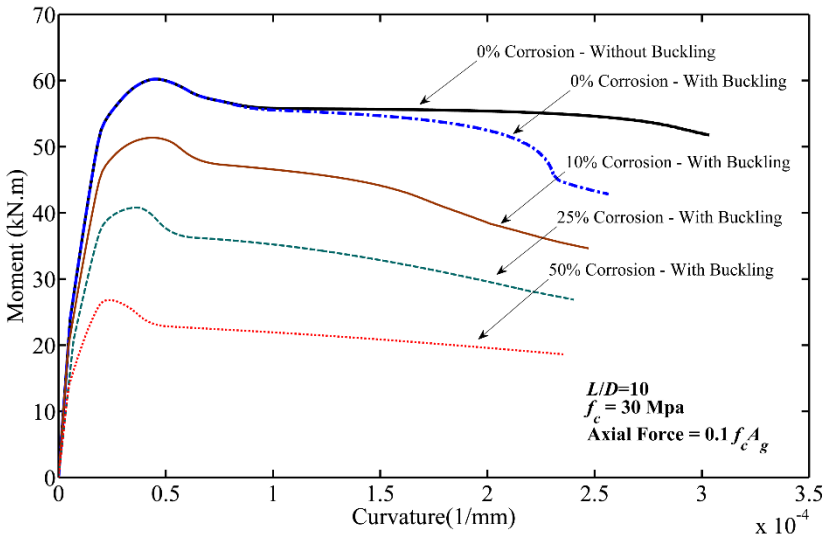

(a)

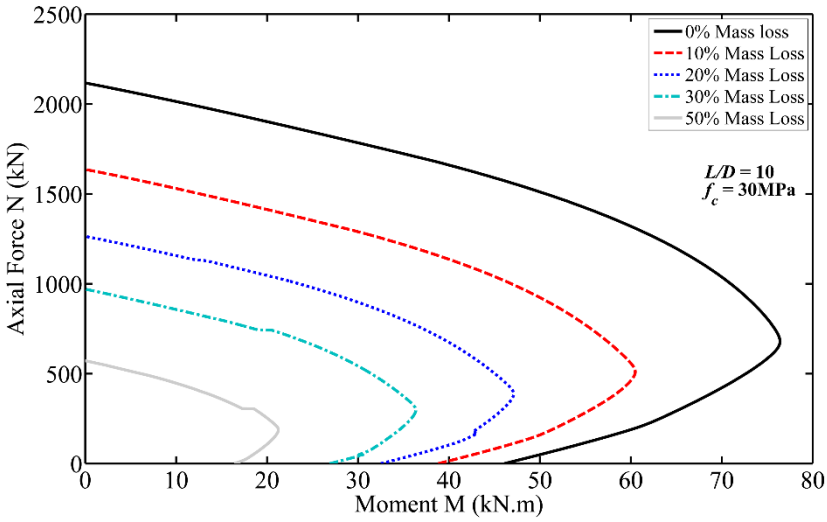

(b)

Figure 8 Impact of corrosion on inelastic response of RC section: (a) Moment-curvature response and (b) axial force - bending moment interaction response

The results of this study show that material degradation has a significant impact on the nonlinear response of RC structures at section and component level. This will subsequently affect the system response i.e. response of a whole bridge subject to increased live load over the service life and/or earthquake loading. Therefore, considering only a uniform area loss of reinforcing bars in structural evaluation of corrosion damaged bridges in both seismic and non-seismic regions is not a sufficiently accurate. The assessment methodology and guidelines developed in this paper, significantly improve on previous methods. Moreover, the computer code is relatively simple and can be implemented in any standard section analysis software or engineering spreadsheets to be used in industry. However, there is still need for further experimental studies on corroded RC components for further validation and calibration of this model under various loading protocols and corrosion scenarios. Nevertheless, this method is currently the only available and reliable computational platform for prediction of the residual capacity of corrosion damaged RC columns/bridge piers.

6. Conclusions

The outcome of this study resulted in a significant improvement to the existing models for the structural evaluation and seismic assessment of corrosion damaged RC bridge piers. The new uniaxial material models have enhanced the accuracy of nonlinear beam-column models for predicting the nonlinear response of RC sections and columns.

The main outcomes of this study can be summarised as follows:

1) The results of this study show that it is inadequate to assume that corrosion only affects the main vertical reinforcement in the column. It was found that the confined concrete with corroded confinement reinforcement starts crushing much faster than uncorroded undamaged concrete. This change in the failure mode cannot be predicted if the damage in core confined concrete due to corrosion of tie reinforcement is ignored.
2) Corrosion induced damage to horizontal tie reinforcement results in premature buckling of the vertical reinforcement. This is in good agreement with observed experimental results reported by other researchers (Meda et al., 2014; Ma et al., 2012). The computational platform developed in this paper is capable of predicting this failure mode.
3) The results of numerical analyses of uncorroded and corroded RC column sections showed that inelastic buckling of vertical bars changes the failure mode of columns subject to lateral loading. In the absence of buckling the failure mode is governed by fracture of bars in tension. However, inelastic buckling of vertical bars results in premature crushing of core concrete. Therefore, the failure mode is governed by crushing of core concrete in compression. It should be noted that the level of axial force applied to the column is also important which is included in the proposed numerical model.
4) The modelling technique developed in this paper has significantly improved the earlier models and can be used by other researchers and practicing engineers for structural capacity assessment and evaluation of corrosion damaged RC columns and sections.

Acknowledgement

The experimental work is funded by the Earthquake Engineering Research Centre (EERC) of the University of Bristol. Any findings, opinions and recommendations provided in this paper are only based on the author's view.

References

Alipour A, Shafei B and Shinozuka M (2011) Performance evaluation of deteriorating highway bridges located in high seismic areas. Journal of Bridge Engineering 6 (5): 597-611

Apostolopoulos CA (2007) Mechanical behavior of corroded reinforcing steel bars S500s tempcore under low cycle fatigue. Construction and Building Materials 21: 1447–1456.

Apostolopoulos CA, Papadopoulos MP and Pantelakis SG (2006) Tensile behavior of corroded reinforcing steel bars BSt 500s. Construction and Building Materials 20: 782–789.

Aquino W (2002) Long-term Performance of Seismically Rehabilitated Corrosion-Damaged Columns. PhD Thesis University of Illinois at Urbana-Champaign.

American Society of Civil Engineers (2013) Report Card for America's Infrastructure. http://www.infrastructurereportcard.org/a/#p/bridges.

Balan TA, Filippou FC and Popov EP (1998) Hysteretic model of ordinary and high-strength reinforcing steel. Journal of Structural Engineering 124 (3): 288–297.

Bathe KJ (1996) Finite element procedure. Prentice Hall, New Jersey, USA.

Broomfield JP (2007) Corrosion of Steel in Concrete. Second Edition Taylor and Francis.

Cairns J, Plizzari GA, Du YG, Law DW and Chiara F (2005) Mechanical properties of corrosion-damaged reinforcement. ACI Material Journal 102 (4): 256–264.

Choe D, Gardoni P, Rosowsky D and Haukaas T (2008) Probabilistic capacity models and seismic fragility estimates for RC columns subject to corrosion. Reliability Engineering & System Safety 93: 383–393.

Coronelli D and Gambarova P (2004) Structural Assessment of Corroded Reinforced Concrete Beams: Modelling Guidelines. Journal of Structural Engineering 130(8): 1214-1224.

Cox WJE (2000) PhD. Nonlinear analysis of reinforced concrete portal frames. University of East London to be submitted

Dhakal R and Maekawa K (2002) Modeling for postyield buckling of reinforcement. Journal of Structural Engineering 128(9): 1139–1147.

Du YG, Clark LA and Chan AHC (2005a) Residual capacity of corroded reinforcing bars. Magazine of Concrete Research 57(3): 135–147.

Du YG, Clark LA and Chan AHC (2005b) Effect of corrosion on ductility of reinforcing bars. Magazine of Concrete Research 57 (7): 407–419.

Ghosh J and Padgett JE (2010) Aging considerations in the development of time- dependent seismic fragility curves. Journal of Structural Engineering 136 (12): 1497–1511.

Hida S et al. (2010) Assuring bridge safety and serviceability in Europe. Technical report No. FHWA-PL-10-014: Office of International Programs Federal Highway Administration US Department of Transportation American Association of State Highway and Transportation Officials.

Hill CD, Blandford GE and Wang ST (1989) Post-buckling analysis of steel space trusses. Journal of Structural Engineering 115 (4): 900-919.

Kashani MM (2014) Seismic Performance of Corroded RC Bridge Piers: Development of a Multi-Mechanical Nonlinear Fibre Beam-Column Model. PhD Thesis University of Bristol.

Kashani MM, Crewe AJ and Alexander NA (2013a) Nonlinear stress-strain behaviour of corrosion-damaged reinforcing bars including inelastic buckling. Engineering Structure 48: 417–429.

Kashani MM, Crewe AJ and Alexander NA (2013b) Nonlinear cyclic response of corrosion-damaged reinforcing bars with the effect of buckling. Construction and Building Materials 41: 388-400.

Kashani MM, Crewe AJ and Alexander NA (2013c) Use of a 3D optical measurement technique for stochastic corrosion pattern analysis of reinforcing bars subjected to accelerated corrosion. Corrosion Science 73: 208-221.

Kashani MM, Lowes LN, Crewe AJ and Alexander NA (2014) Finite element investigation of the influence of corrosion pattern on inelastic buckling and cyclic response of corroded reinforcing bars. Engineering Structures 75: 113-125.

Kashani MM, Lowes LN, Crewe AJ and Alexander NA (2015a) Phenomenological hysteretic model for corroded reinforcing bars including inelastic buckling and low-cycle fatigue degradation'. Computers and Structures 156: 58-71.

Kashani MM, Alagheband P, Khan R and Davis S (2015b) Impact of corrosion on low-cycle fatigue degradation of reinforcing bars with the effect of inelastic buckling. International Journal of Fatigue 77: 174-185.

Kashani, MM, Barmi AK, and Malinova VS (2015c). Influence of inelastic buckling on low-cycle fatigue degradation of reinforcing bars. Construction and Building Materials 94: 644-655.

Lehman DE and Moehle JP (2000) Seismic performance of well-confined concrete columns. PEER Research Report University of California at Berkeley.

Lowes LN, and Altoontash A (2003) Modeling reinforced-concrete beam-column joints subjected to cyclic loading. Journal of Structural Engineering 129 (12): 1686-1697.

Ma Y, Che Y and Gong J (2012) Behavior of Corrosion Damaged Circular Reinforced Concrete Columns under Cyclic Loading. Construction and Building Materials 29: 548–556.

Meda A, Mostosi S, Rinaldi Z and Riva P (2014) Experimental evaluation of the corrosion influence on the cyclic behaviour of RC columns. Engineering Structures 76: 112-123.

McGuire W, Gallagher RH, Ziemian RD (2000) Matrix structural analysis. John Wiley and Sons, USA.

Noor FA, Alexander NA and Cox WJE (2000) Developing a Non-Linear Analysis Method for Reinforced Concrete Frames. Proceedings of the 10th Annual British Cement Association conference, Birmingham, UK.

OpenSees, The Open System for Earthquake Engineering Simulation (2014) PEER, University of California, Berkeley, USA.

Park R, Priestley N and Gill W (1982) Ductility of Square-Confined Concrete Columns. Journal of Structural Division 108 (4): 929-951.

Scott BD, Park R and Priestley MJN (1982) Stress-strain behavior of concrete confined by overlapping hoops at low and high strain rates. ACI Journal 79 (1): 13-27.

Spacone E, Filippou FC and Taucer FF (1996a) Fibre beam-column model for non-linear analysis of R/C frames: Part I. Earthquake Engineering and Structural Dynamics 25(7): 711-726.

Spacone E, Filippou FC and Taucer FF (1996b) Fibre beam-column model for non-linear analysis of R/C frames: Part II. Applications. Earthquake Engineering and Structural Dynamics 25(7): 727-742.

Thai HT and Kim SE (2011) Nonlinear inelastic time-history analysis of truss structures, Journal of Constructional Steel Research 67: 1966-1972.

Vecchio FJ and Collins MP (1986) The modified compression-field theory for reinforced concrete elements subjected to shear. ACI Journal 83 (2): 219-231.

Wallbank EJ (1989) The performance of concrete in bridges: A survey of 200 highway bridges, London.